



OPEN Novel processing algorithms for efficient dam seepage surveys via improved symmetric multielectrode electrical exploration

Duc Minh Vu¹✉, Anh Chung Do² & Gómez-Ortiz David^{3,4}✉

To improve the efficiency of geophysical methods, data processing algorithms are often prioritized for enhancement. The novel improved processing and analysis algorithms of the improved multi-electrode electrical exploration methods that we propose include two options: Option 1 and Option 2. In a previous study, the ρ_s^{ct} algorithm (associated with Option 1) was applied to investigate seepage at Dong Do dam in Vietnam, producing structural image with clearly defined geological layer boundaries. To further assess the effectiveness of these data processing algorithms in dam and dike research, the ρ_{pm}^{ct} algorithm (corresponding to Option 2) was applied in this study to survey the same Dong Do dam. The results yielded a resistivity cross-section that revealed differences in horizontal anisotropy and identified blocky anomalies. These findings demonstrate that the application of both algorithms is effective, allowing for comprehensive determination of the dam's structure, as well as the depth and extent of subsurface features. Accordingly, researchers can select either of the two novel data processing options from the improved symmetric multi-electrode electrical exploration method based on the specific objectives and targets of their investigation—while still achieving optimized outcomes.

Keywords Algorithm, Blocky anomalies, Seepage, Dong Do dam, Embankment

Seepage poses a significant threat to the structural integrity and safety of irrigation dams. Unfortunately, it is not always visible externally, making detection and mitigation challenging. When seepage becomes apparent on the surface, it can severely compromise dam stability; however, accurately identifying its precise location remains difficult. As a result, remediation often involves drilling and injecting concrete, a process that is both costly and time-consuming. To address this issue, geophysical methods have been increasingly employed to investigate seepage in dams.

The multi-electrode electrical exploration (MEE) method has proven to be an effective approach^{1–5}. This method has been successfully applied to survey seepage in the Ho Phoi and Dam Bai dams in Hoa Binh province, Vietnam⁶, as well as the right dike of the Chu River in Thanh Hoa province, Vietnam⁷, yielding favorable results.

To enhance the efficiency of constant-current electrical sounding techniques, improved electrical sounding (IES) methods were developed based on conventional one-dimensional (1D) electrode arrays. The fundamental principles and primary advantages of these IES methods have been presented in previous studies^{8,9}.

To leverage the advantages of both the IES and MEE methods, we have integrated them to develop the improved multi-electrode electrical sounding (IMES) method¹⁰, utilizing enhanced one-dimensional (1D) improved multi-electrode arrays. By systematically connecting the electrodes of the improved 1D electrode array to the take-out terminals of the SuperSting device, the enhanced multi-electrode configuration is achieved. These methods have been successfully tested and implemented in practical applications across Vietnam, yielding superior results compared to conventional approaches¹¹. However, it is important to note that both the IES and IMES methods remain limited to 1D surveying.

¹University of Science, Vietnam National University, Hanoi, Vietnam. ²Institute for Ecology and Works Protection, Vietnam Academy for Water Resources, Hanoi, Vietnam. ³Department of Biology and Geology, Physics and Inorganic Chemistry, ESCET, Universidad Rey Juan Carlos, Móstoles, Madrid, Spain. ⁴Research Group 'Geofísica y Geoquímica Ambiental', Universidad Rey Juan Carlos, Móstoles, Spain. ✉email: vducminh56@gmail.com; minhvd@vnu.edu.vn; david.gomez@urjc.es

The advantages of the IES, IMES and MEE methods have been integrated to develop the Improved Multi-electrode Electrical Exploration (IMEE) methods^{12,13}, which encompass both resistivity and induced polarization techniques. These methods utilize enhanced two-dimensional (2D) improved multi-electrode arrays, enabling faster measurements compared to conventional approaches. To date, these methods have been fully developed in terms of survey design, data collection, measurement process control file configuration, and algorithms and programs for processing and analyzing. However, the Improved Petrovski parameter processing algorithms remain incomplete.

The IMEE methods offer significant advantages over previous approaches, as they incorporate simple algebraic calculations to determine resistivity and polarization values across different electrode arrays—including the Improved Petrovski parameter with enhanced resolution. These calculations can be performed even when using any improved array, thus overcoming a fundamental limitation of earlier methods: reliance on unstable derivative expressions. The proposed advancements exhibit high scientific reliability, substantial practical utility, and considerable significance in both theoretical and applied research.

A detailed introduction to the IMEE methods, along with selected results from modeling, experimentation, and practical applications in Vietnam—demonstrating improved performance compared to earlier approaches—has been presented in previous publications^{12–16}.

The improved symmetric multi-electrode electrical exploration (ISMEE) method is a component of the IMEE method system. Its newly developed data processing algorithms and the effective application results for groundwater survey in Vientiane Province, Laos were introduced the recent publication^{17,18}.

Our proposed improved data processing and analysis algorithms for the IMEE methods include two alternatives—Option 1 and Option 2—which will be detailed in the Methodology section. The application of the ISMEE method utilizing the improved data processing algorithm based on Option 1 (main parameter ρ_s^{ct}) for seepage survey at Dong Do dam in Vietnam have yielded a detailed and well-defined structural image, characterized by smooth and distinct geological layer boundaries¹⁹.

This study primarily provides a briefly introducing to the newly improved processing and analysis algorithms of the ISMEE method based on Option 2 (with the main parameter ρ_{pm}^{ct}), along with their application in surveying seepage at the same Dong Do dam in Vietnam. The results from the research area have been processed and presented using both Option 1 and Option 2 of the newly improved algorithms to facilitate a comparative evaluation of their effectiveness.

Methodology

As stated in the introduction, the IMEE methods, which utilize enhanced two-dimensional (2D) multi-electrode arrays, have been developed through the integration and refinement of the IRS and MEE methods. Consequently, the IMEE methods inherit all the advantages of both IRS and MEE approaches.

The IMEE methods we have proposed, along with their effective application results, have been introduced in previously cited studies (as referenced in the introduction). This section provides a concise overview of the ISMEE method, with a particular emphasis on the calculation formulas for key parameters and the block diagram of its newly improved data processing algorithms. This serves as a foundational basis for presenting its application results in the seepage survey at the Dong Do dam in the subsequent sections.

For the first time, the improved Petrovski parameters have been proposed with a well-defined scientific theoretical foundation.

The ISMEE method follows the same measurement procedure as the traditional MEE method, utilizing a control file created by the authors and installed in the measuring device. However, an improved symmetric multi-electrode array has been developed based on the following principles: A and B serve as the current-injecting electrodes, M and N function as the potential-measuring electrodes, and MA represents the separation between the M and A electrodes. It is important to note that the principle of reciprocity in electrical sounding has been applied, requiring the current-injecting electrodes to be positioned internally.

$$MA = AB = BN = n.a$$

$$MA = 4AB = BN = 4n.a \text{ (extended receiver)}$$

$$MA = AB = BN = 3n.a \text{ (extended transmitter)}$$

where a represents the constant distance between adjacent electrodes, n denotes the n th measurement for each configuration listed above.

By conducting measurements using the improved symmetric multi-electrode array, all essential information can be obtained after processing the collected data.

The data conversion and key parameter calculation formulas are developed based on the transformation principles of the IRS methods, with the primary distinction being that the conversion formulas can be applied to all acquired resistivity data. A major advantage of the data processing and analysis algorithms in the ISMEE method is their reliance on simple and robust algebraic formulas, eliminating the need for unstable derivative-based calculations used in previous approaches.

The newly improved processing algorithms of the ISMEE method consist of two options:

Option 1: Calculate the improved symmetrical resistivity values ρ_s^{ct} derived from the ISMEE method. These ρ_s^{ct} values are subsequently processed, analyzed and visualized using AGI EarthImager 2D software²⁰, Version 2.4.2 (Buil 627), (EI Usergroup URL: <https://www.agiusa.com/files/eicust/earthimageruser.shtml>).

Option 2: Calculate the improved parameters based on the proposed algorithm, with a particular focus on the newly improved Petrovski resistivity values $\rho_{pm, sr}^{ct}$. The results obtained from the calculation and anal-

ysis process will be visualized using EarthImager 2D software; however, the Petrovski resistivity values are presented separately using Surfer software (Surfer 29.1.267 (64 bit) Mar 1 2025 (Free Trial), Copyright @ 1993–2025 Golden Software. LLC, <https://www.goldensoftware.com/products/>).

The formulas for calculating the main parameters¹⁸: with one generating electrode separation (AB)_p, where the resistivity values $\rho_s^{ct}(i)$ and $\rho_s^{ct}(i+1)$ corresponding to r_i and r_{i+1} obtained from the field measurements. The average values ρ_s^{ct} are calculated using the following formula:

$$\rho_{sj}^{ct}(i) = \sqrt{\rho_s^{ct}(i) \cdot \rho_s^{ct}(i+1)} \quad (1)$$

The values ρ_{sr}^{ct} are calculated from the values ρ_s^{ct} according to the following formula:

$$\rho_{srj}^{ct}(i) = \left| \frac{1}{2} K_r \left(\left(\frac{\rho_{sj}^{ct}(i+1)}{K_s(i+1)} - \frac{\rho_{sj}^{ct}(i)}{K_s(i)} \right) \right) \right| \quad (2)$$

where K_r represents the coefficient of the improved dipole-axis multi-electrode array; K_s denotes the coefficient of the improved symmetrical multi-electrode array.

The newly improved Petrovski values $\rho_{pm, sr}^{ct}$ are proposed according to the following formula:

$$\rho_{pm, srj}^{ct}(i) = \rho_{sj}^{ct}(i) / (2\rho_{srj}^{ct}(i) / \rho_{sj}^{ct}(i) - 1) = \rho_{sj}^{ct}(i) \cdot f(x) \quad (3)$$

in there: the functions $f(x)$, where the variable x is defined as $x = \frac{2\rho_{srj}^{ct}(i)}{\rho_{sj}^{ct}(i)}$, is built to overcome discontinuities and negative values observed in previous Petrovski curves:

$$f(x) = \begin{cases} \frac{1}{x-1} & \text{when } x \geq 1.025 \\ ax + b + \frac{c}{x} & \text{when } 0 < x < 1.025 \end{cases} \quad (4)$$

with conditions: $f_1(1.025) = f_2(1.025)$, $f_1'(1.025) = f_2'(1.025)$, $f_1''(1.025) = f_2''(1.025)$. This ensures that the values $\rho_{pm, sr}^{ct}$ will be continuous and non-negative, overcoming the disadvantage of the previous Petrovski parameter.

In the formulas (1), (2) and (3), the index i represents i th extension of the generating electrodes distance r_i for a given sounding point, while index j denotes the corresponding sounding points.

The block diagram illustrating the newly improved processing algorithms of the ISMEE method, as implemented in our programs is presented in Fig. 1.

Research area and the survey profiles

The selected research area is Minh Tri commune, Soc Son district, Hanoi, Vietnam. Minh Tri commune is located in geographical coordinates 105°45'56" to 105°46'40" East longitude and 21°18'36" to 21°19'36" North latitude (Fig. 2).

Based on the 1:50,000-scale geological map of Hanoi published²¹, along with results from borehole investigations, the main stratigraphic units identified in the study area are as follows: The uppermost layer consists of recent alluvial deposits, including clay, silty clay, sandy silt, and sand. These materials are widely distributed across the study area's surface and belong to the Thai Binh Formation (aQ²³tb). The middle layer is composed of coastal marsh and lacustrine deposits, featuring clay, silty clay, sandy silt, and sand, which are classified under the Hai Hung Formation (ambQ²¹⁻²hh). Beneath this lies a layer of lacustrine-marsh and fluvial deposits, primarily composed of clay, silty clay, sandy silt, and sand, identified as the Vinh Phuc Formation (aQ¹³vp). Further below, floodplain and river deposits—including clay, silty clay, sand, and gravel—are assigned to the Hanoi Formation (ap, aQ¹²⁻³hn). Additionally, weathering products from the bedrock, predominantly silty sandstone, manifest as reddish-brown clay and silt with mottled gray-yellow to gray-white hues (deQ). However, these materials are present only in limited areas and are not discussed in detail within this report.

Geological conditions²²: The Dong Do dam site comprises multiple soil layers. The uppermost layer consists of embankment fill, with thicknesses varying from 1.5 m to 18.25 m depending on location. Beneath this lies Layer 2, composed of silty clay interspersed with gravel and cobbles, exhibiting a soft to plastic consistency, moderate bearing capacity, and deformability. Layer 3 consists of stiff to semi-hard silty clay, which has relatively good bearing capacity and low compressibility. The deepest section consists of strongly to completely weathered argillaceous rocks, transitioning into moderately weathered argillaceous rocks—these layers provide good bearing capacity with minimal deformability. Dam body: The main constituent material is silty clay mixed with gravel and cobbles, characterized by moderate permeability, with an in-situ permeability coefficient of $K = 3.40 \times 10^{-4}$ cm/s. Additionally, localized site investigations revealed signs of water loss within this soil layer. Dam foundation: Layers 2 and 3, composed of silty clay, also exhibit moderate permeability, with in-situ permeability coefficients of $K = 1.43 \times 10^{-4}$ cm/s and $K = 9.33 \times 10^{-5}$ cm/s, respectively. Underlying these are fully to strongly-moderately weathered sandstone and siltstone, which are characterized by low permeability.

Three resistivity profiles were surveyed on Dong Do dam in the mentioned study area above, using the ISMEE method with the improved symmetrical multi-electrode array, utilizing the device SUPERSTING R8/IP + 56 poles from AGI (USA)²³. The profiles were taken from the left shoulder to the right shoulder of the dam, with a distance of 3 m between measuring points. The length of the dam surface profile is 249 m, while the central profile of roof 1 spans 219 m and that of roof 2 covers 165 m (Fig. 2).

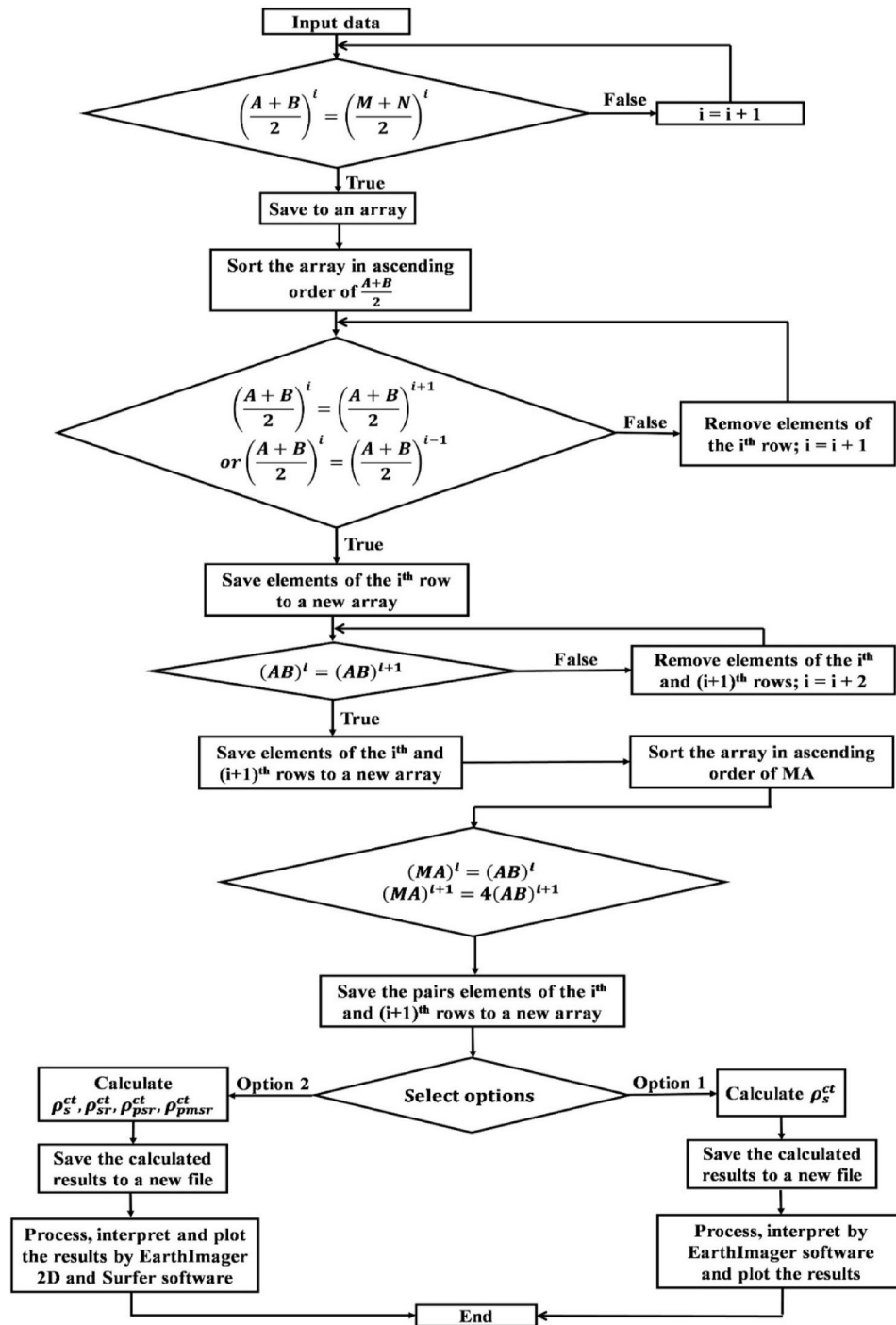


Fig. 1. The block diagram of the newly improved processing algorithms.

Survey results

The data processing results obtained from implementation of the ISMEE method at Dong Do dam are shown in the following figures, corresponding to the two options described above.

Profile along the middle of the dam surface

The processing results for this profile are presented in Fig. 3, illustrating two options.

Option 1 (Fig. 3a): The dam structure comprises three distinct layers. Layer 1 is thin with low resistivity, Layer 2 is thicker and exhibits higher resistivity, Layer 3 is the thickest layer—displays significant resistivity fluctuations. Notably, two low-resistivity anomalies are observed, potentially indicating unusual seepage phenomena within the dam.

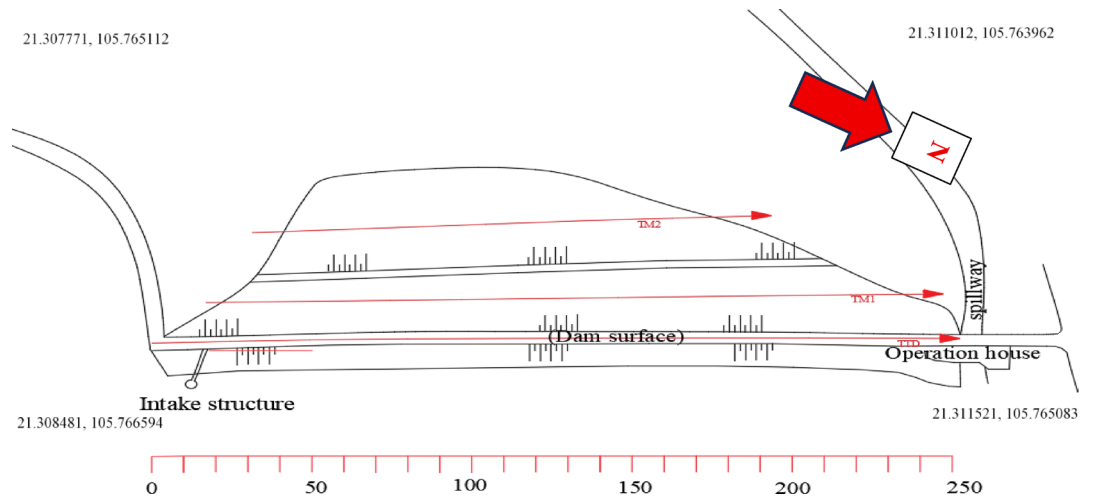


Fig. 2. Location of survey profiles on the Dong Do dam (visualized with the software: Surfer 29.1.267 (64 bit) Mar 1 2025 (Free Trial), Copyright @ 1993–2025 Golden Software. LLC, <https://www.goldensoftware.com/products/>).

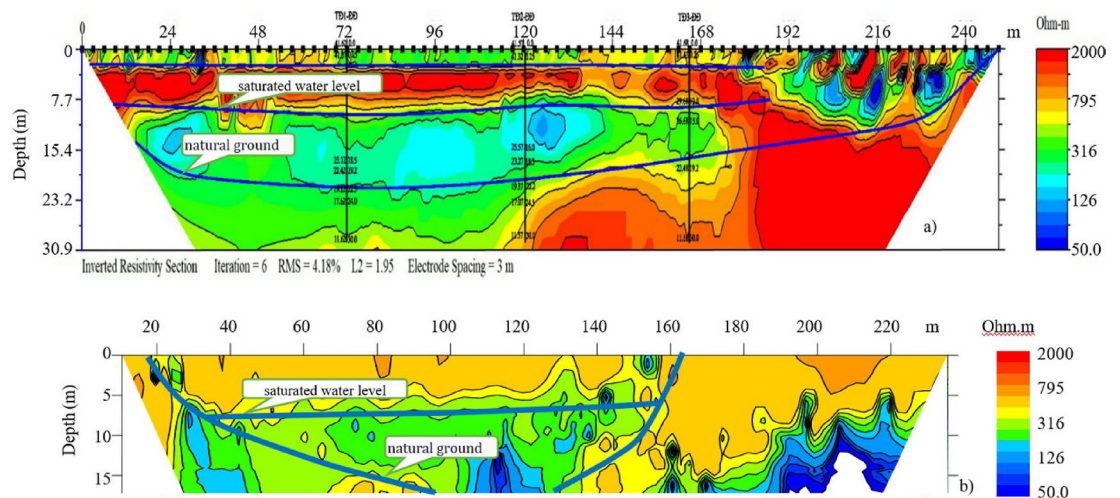


Fig. 3. Resistivity cross-sections of profile along the middle of the surface of the Dong Do dam (a) Results of processing ρ_s^{ct} (option 1)¹⁹; (b) Results of processing ρ_{pm}^{ct} (option 2).

Option 2 (Fig. 3b): These results highlight the saturated water level and the dam foundation. However, compared to Option 1, the topmost low-resistivity layer is absent. Instead, a seepage anomaly is detected at the beginning of the profile, spanning from the 22nd to the 40th meter. This suggests that the anomaly has shifted by approximately 4 meters relative to the results obtained in Option 1.

Central profile of roof 1

The processing results for this profile, based on the two analytical options, are presented in Fig. 4.

Option 1 (Fig. 4a): The upper layers contain one fewer layer than the profile along the middle of the dam surface:

- Layer 1: This layer extends throughout the survey line with a resistivity greater than 1,000 Ωm at depths ranging from 0 m to 4.5 m. It represents the boundary of the saturated water level within the dam body.
- Layer 2: The depth extends from 4.5 m to 15 m, marking the boundary between the embankment and the natural ground of the dam. At depths between 3 to 8 m, from the starting point to the 30th meter of the section, a low-resistivity anomaly of approximately 150 Ωm is observed. Notably, this anomaly is surrounded by a medium with a resistivity exceeding 800 Ωm , indicating a potential seepage anomaly within the dam.

The results obtained using Option 2 (Fig. 4b) indicate that:

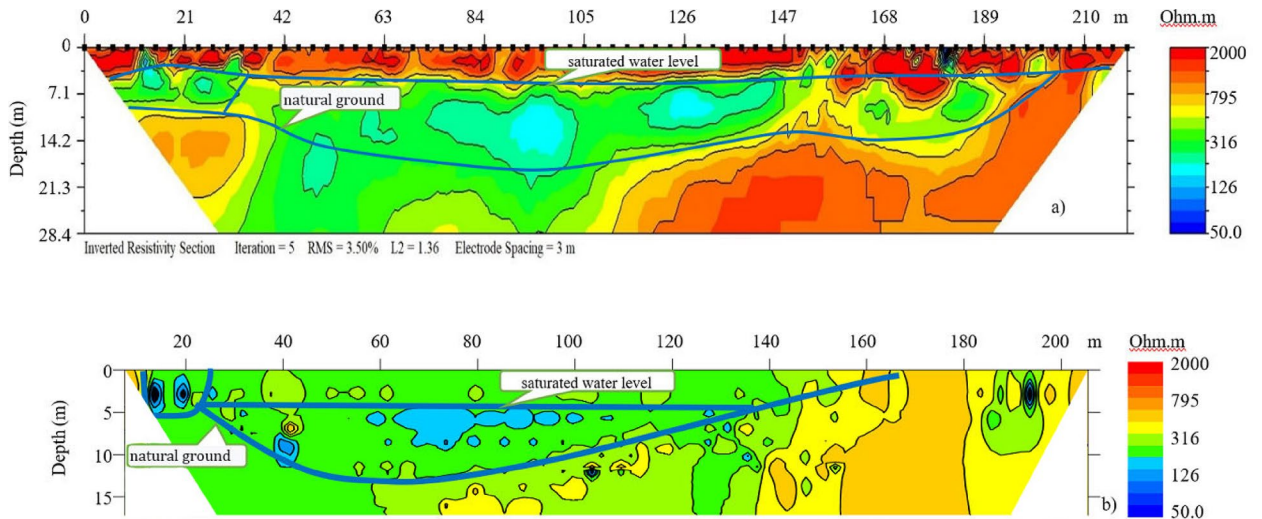


Fig. 4. Resistivity cross-sections of the central profile of roof 1 of the Dong Do dam (a) Results of processing ρ_s^{ct} (option 1)¹⁹; (b) Results of processing ρ_{pm}^{ct} (option 2).

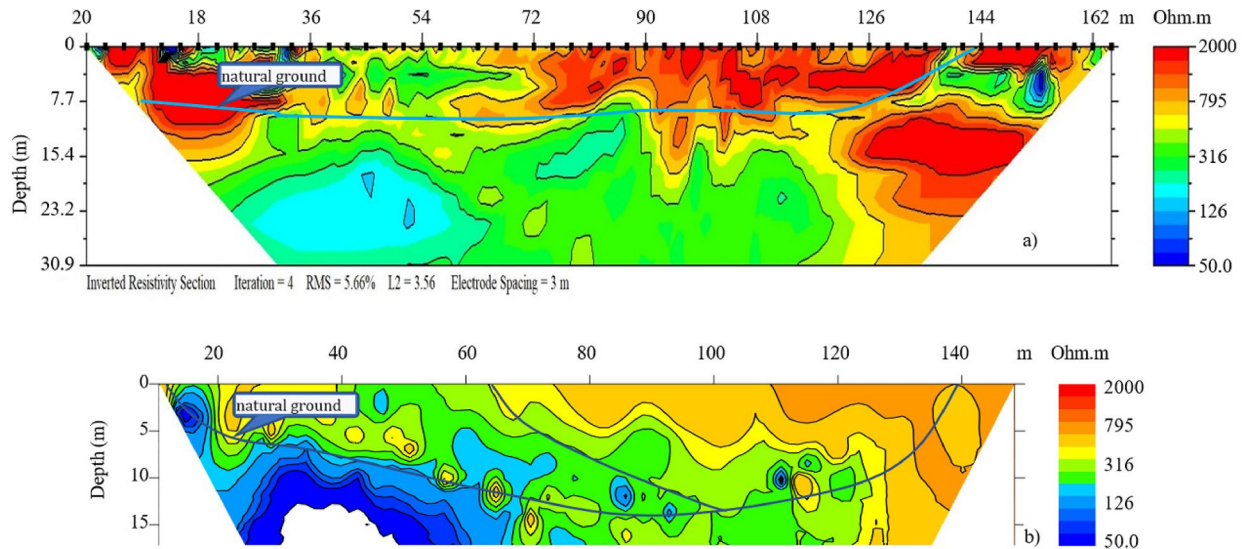


Fig. 5. Resistivity cross-sections of the central profile of roof 2 of the Dong Do dam (a) Results of processing ρ_s^{ct} (option 1)¹⁹; (b) Results of processing ρ_{pm}^{ct} (option 2).

- Saturated Water Level: The saturated water level within the dam body reaches a depth of approximately 4 m. However, it is noteworthy that the saturated water level is flat compared to the results observed in Option 1.
- Boundary Definition: The boundary between the dam body and the dam foundation is clearly defined, extending to a depth of 15 m.
- Resistivity Anomaly: Within the first 30 m of the profile, the low resistivity anomaly is significantly more pronounced than in Option 1. This suggests a potential seepage occurring at the dam shoulder.

Central profile of roof 2

The processing results for this profile are presented in Fig. 5.

Option 1 (Fig. 5a): The processed ρ_s^{ct} values for the central profile of roof 2 reveal the presence of two distinct layers: the embankment and the foundation. The embankment has an estimated thickness of approximately 8 m. Notably, between meter 12 and meter 65 of the survey section, a low-resistivity anomaly emerges from the surface. This suggests the potential for seepage at the dam face, particularly when the lake water level rises.

Option 2 (Fig. 5b): The results indicate the presence of the saturated water level, floating seepage on the dam surface, and the junction between the dam body and foundation, occurring at a depth of approximately 4 m. However, compared to Option 1, the saturated water level does not exhibit the same uniform flatness.

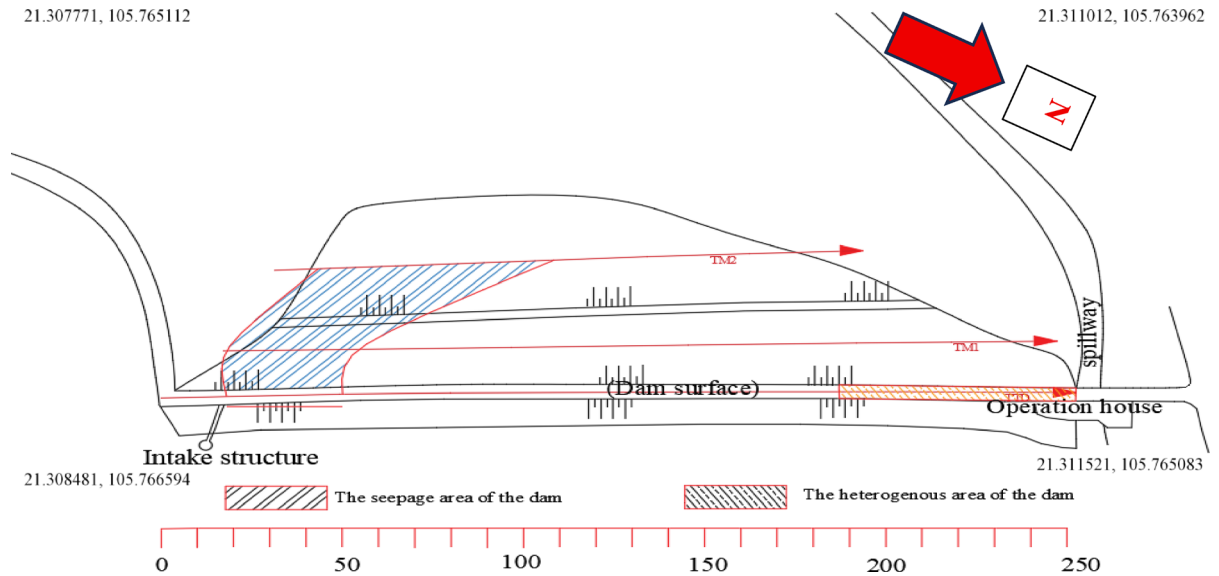


Fig. 6. Location of the seepage and heterogeneous areas on the Dong Do dam (visualized with the software: Surfer 29.1.267 (64 bit) Mar 1 2025 (Free Trial), Copyright @ 1993–2025 Golden Software. LLC, <https://www.goldensoftware.com/products/>).

A comparison between the results obtained using the ISMEE method and those derived from pre-existing boreholes²⁴ demonstrates a consistent agreement. Based on the survey findings, the current status of Dong Do dam is illustrated in Fig. 6.

Discussion

The newly data processing algorithms of the ISMEE method are developed based on the continuous improvement of the (1D) improved electrical sounding method which was also proposed by us. The enhanced algorithms offers two data processing options, allowing researchers to choose the most suitable approach depending on the specific objects and objectives of their study, while still achieving satisfactory results.

In short, utilizing the ISMEE method with the newly improved processing algorithms proves to be more effective than older methods, as it provides a comprehensive and detailed representation of the study environment.

Conducting three survey lines at Dong Do dam using the ISMEE method with newly improved processing algorithms is entirely feasible. This approach yields highly reliable results in detecting changes in the embankment caused by seepage or other heterogeneities that may lead to dam disturbance.

The survey results provide essential insights into the embankment, including its layering, the depth and extent of the seepage area, and the presence of heterogeneities within the dam:

- The resistivity cross-section along the middle of the dam surface reveals that the area extending from the left shoulder to the 185th meter consists of three distinct layers. In contrast, the central section of Roof 1 contains one fewer layer than of profile along the middle of the dam surface. Additionally, the central section of Roof 2 exhibits only two layers, which enhances the visibility of the boundary between the embankment and the foundation.
- Across all three sections of the dam, survey results have shown the presence of a low-resistivity anomaly on the left shoulder. This anomaly may be the underlying cause of seepage from upstream to downstream, suggesting the potential for surface seepage when the lake water level rises.
- Heterogeneous areas have been identified at depths from the dam surface down to 11 m, as well as near the spillway.

Conclusions

Based on the processing results obtained from the two analytical options, we have reached the following conclusions:

Using Option 1, the structural representation of the environment is depicted more clearly in the resistivity cross-sections, with flatter layer boundaries compared to Option 2. Therefore, applying the processing and analyzing algorithm to the parameter ρ_s^{ct} of the ISMEE method yields more accurate results in environments characterized by horizontal layering or have horizontally elongated objects.

Using option 2, the application of the processing and analyzing algorithm to the improved Petrovski parameter ρ_{pm}^{ct} reveals indications of stratification. However, compared to Option 1, the saturated water level is less uniform, and the topmost low-resistivity layer is absent. These results produce a resistivity cross-section accentuates variations in horizontal heterogeneities or blocky anomalies. Therefore, the processing and analysis

algorithm in Option 2 of the ISMEE method proves more effective in environments that lack layering or contain cubic objects.

The findings presented above confirm the effectiveness of the newly improved processing algorithms of the ISMEE method. Furthermore, these algorithms provide the flexibility to choose between two processing options, allowing researchers to tailor the approach based on the objectives and specific characteristics of their study. This enhances the efficiency of the processing workflow while ensuring optimal results. Therefore, these algorithms can be applied not only for detecting seepage areas, but also for identifying potential hazards in dams—even when no visible signs of deterioration are present.

Data availability

Data is provided within the manuscript.

Received: 15 April 2025; Accepted: 19 August 2025

Published online: 26 September 2025

References

1. Yilmaz, S., Okyar, M. & Gurbuz, M. Electrical resistivity imaging for investigation of seepage paths in the Yukari Gökdere Dam, Isparta, Turkey. *Bull. Eng. Geol. Env.* **80**, 115–125. <https://doi.org/10.1007/s10064-020-01952-2> (2021).
2. Fata, Y. A., Suhartanto, E., Hendrayanto, H., Rubiantoro, P. Seepage patterns in an earth-rock fill dam evaluation using electrical resistivity tomography (ERT) method. in *IOP Conference Series: Earth and Environmental Science, 4th International Conference of Water Resources Development and Environmental Protection (ICWRDEP 2021) 7 August, Malang, Indonesia (Virtual)* **930**, 012090. <https://doi.org/10.1088/1755-1315/930/1/012090> (2021).
3. Guo, Y. et al. Seepage detection in earth-filled dam from self-potential and electrical resistivity tomography. *Eng. Geol.* **306**, 106750. <https://doi.org/10.1016/j.enggeo.2022.106750> (2022).
4. Li, J., Chen, C., Wu, Z. & Chen, J. Multi-source data-driven unsaturated seepage parameter inversion: Application to a high core rockfill dam. *J. Hydrol.* **617**, 129171. <https://doi.org/10.1016/j.jhydrol.2023.129171> (2023).
5. AL-Mahemmdi, W. D., Al-Banna, A. S. & AL-Menshed, F. H. Detection of A possible subsurface water seepage using 2D electrical resistivity imaging survey at a site in Al-Khwarizmi College of Engineering, University of Baghdad, Iraq. *Iraqi. J. Sci.* **64**(4), 1810–1819. <https://doi.org/10.24996/ijs.2023.64.4.21> (2023).
6. Do, C. A., Vu, M. D. & Eldosouky, A. Some initial study results of determining seepage area in the earth dam of reservoirs. *VNU. J. Sci. Nat. Sci. Technol.* **27**(3): 154–166. (2011)
7. Do, C. A. & Vu, M. D. Survey on seepage in dikes with the Multi-electrode Resistivity Imaging method. *VNU. Journal of Science, Natural Sciences and Technology* **28**(1), 11–18. <https://js.vnu.edu.vn/NST/article/view/1167> (2012). (in Vietnamese)
8. Le-Viet, K. D. & Vu, M. D. A new method by using the reasonable combination of electrode array for resistivity sounding. *J. Sci. Earth* **23**(3), 217–224 (2001) ((in Vietnamese)).
9. Vu, M. D. Induced-polarization sounding methods in a new manner. *J. Geol.* **17–18** (Series B), 94–101 (2001).
10. Vu, M. D. The Improved Multi-electrode Electrical Sounding Method. *VNU. J. Sci. Nat. Sci. Technol.* **26**(4), 233–241. <https://js.vnu.edu.vn/NST/article/view/1983> (2010).
11. Vu, M. D. & Do, C. A. Study of seepage area models in dams and dikes by the Improved Multi-electrode Resistivity Imaging and Ground Penetrating Radar. *VNU. J. Sci. Nat. Sci. Technol.* **29**(3), 30–39. <https://js.vnu.edu.vn/NST/article/view/1041> (2013). (in Vietnamese)
12. Vu, M. D. & Do, C. A. Introduction to the advanced multi-electrode electrical sounding method. *VNU. J. Math. Phys.* **31**(3), 1–14. <https://js.vnu.edu.vn/Map/article/view/112> (2015a).
13. Vu, M. D. & Do, C. A. Perfecting the advanced multi-electrode electrical sounding method. *VNU. J. Math. Phys.* **34**(3), 90–103. <https://doi.org/10.25073/2588-1124/vnumap.4291> (2018).
14. Vu, M. D. & Do, C. A. Some experiment results of determining saturation line in Dong Mo dam by the Advanced Multi-electrode Electrical Sounding Method. *VNU. J. Sci. Nat. Sci. Technol.* **31**(3), 23–37. (2015b) (in Vietnamese)
15. Vu, M. D. Application of interpolation algorithm in data processing of the advanced multi-electrode electrical sounding method to determine saturation line in the earth dam. *VNU. J. Sci. Math. Phys.* **32**(3), 86–95. <https://doi.org/10.25073/2588-1124/vnumap.4056> (2016).
16. Do, C. A. & Vu, M. D. Application of the advanced 2D multi-electrode electrical exploration method in surveying Dyke's current condition and its contribution to assessing the stability of Dyke. *VNU. J. Sci. Nat. Sci. Technol.* **35**(1), 104–118 (2019).
17. Vu, M. D. et al. Application of the improved multi-electrode electrical exploration methods for groundwater investigation in Vientiane Province, Laos. *J. Asian Earth Sci.* **X** 5, 100056. <https://doi.org/10.1016/j.jaesx.2021.100056> (2021).
18. Vu, M. D. et al. A new algorithm for processing data of the improved multi-electrode electrical exploration method: Application to groundwater investigation. *Acta Geophys.* **72**, 2555–2563. <https://doi.org/10.1007/s11600-023-01244-9> (2024).
19. Do, C. A., Vu, M. D., Pham, L. T. & Eldosouky, A. M. Surveying the seepage area in the Dong Do dam by the improved multi-electrode electrical exploration method. *Front. Sci. Res. Technol.* **3**, 70–77. <https://doi.org/10.21608/frst.2021.112247.1053> (2022).
20. Advanced Geosciences, Inc. *Instruction manual for EarthImager 2D, Version 2.4.2, Resistivity and IP Inversion Software*; Austin, Texas 78726, USA (2002–2009).
21. Dao, V. T. et al. Geological and mineral map content at 1:50,000 scale of the expanded Hanoi City area. *J. Geol. Ser. A*, **351**, 1–10. <https://journalofgeology.vn/index.php/home/article/view/467> (2015). (in Vietnamese).
22. Institute of Water Resources Engineering. *Assessment of dam and irrigation reservoir safety in Hanoi City in 2021* (Technical report). (2021) (in Vietnamese).
23. Advanced Geosciences, Inc. *Instruction manual for SuperSting™ Earth Resistivity, IP & SP System with Wi-Fi*; Austin, Texas 78726, USA (2013).
24. Institute for Hydraulic Construction. *Geological report on Dong Do dam* (2021). (in Vietnamese)

Author contributions

Duc Minh Vu: methodology, the block diagram and computer program, writing and review. Anh Chung Do: material preparation, data collection and analysis. Gómez-Ortiz David: review. All authors read, reviewed and approved the final manuscript.

Funding

Not applicable.

Declarations

Competing interests

The authors declare no competing interests.

Ethical approval

All authors have read, understood, and complied as applicable with the statement on “Ethical responsibilities of Authors,” as found in the Instructions for Authors.

Additional information

Correspondence and requests for materials should be addressed to D.M.V. or G.-O.D.

Reprints and permissions information is available at www.nature.com/reprints.

Publisher’s note Springer Nature remains neutral with regard to jurisdictional claims in published maps and institutional affiliations.

Open Access This article is licensed under a Creative Commons Attribution-NonCommercial-NoDerivatives 4.0 International License, which permits any non-commercial use, sharing, distribution and reproduction in any medium or format, as long as you give appropriate credit to the original author(s) and the source, provide a link to the Creative Commons licence, and indicate if you modified the licensed material. You do not have permission under this licence to share adapted material derived from this article or parts of it. The images or other third party material in this article are included in the article’s Creative Commons licence, unless indicated otherwise in a credit line to the material. If material is not included in the article’s Creative Commons licence and your intended use is not permitted by statutory regulation or exceeds the permitted use, you will need to obtain permission directly from the copyright holder. To view a copy of this licence, visit <http://creativecommons.org/licenses/by-nc-nd/4.0/>.

© The Author(s) 2025